22nd IAHR International Symposium on Ice
Singapore, August 11 to 15, 2014

Wave Propagation in Frazil/Pancake and Fragmented Ice Covers – Part II: Preliminary Data Analysis

Xin Zhao[1], Christopher Callinan[1] and Hayley Shen[1,*]
1) Department of Civil and Environmental Engineering, Clarkson University, Potsdam, NY, USA
**) Corresponding author: hhshen@clarkson.edu*

Both wavelength and amplitude, as well as the directional distribution of energy, change as waves propagate under ice covers. These changes depend on the wave frequency and the properties of the ice cover. There are several theories for these phenomena, but very limited data to validate these theories. In 2008 a laboratory study at the Hamburgische Schiffbau-Versuchsanstalt GmbH (HSVA) the wave dispersion, including both wavelength change and wave attenuation, was measured for a grease/pancake ice field. The results were compared to those from a grease ice field formed in a smaller wave tank at the University of Washington. It was shown that wave propagation under a grease ice cover followed that of a viscous layer model, but under a pancake ice field they did not. A more extensive study was conducted again in 2013 at HSVA to further investigate the dispersion relationship. These laboratory studies demonstrated their potential to aid the development of wave-ice theories. They can supplement field studies to help characterize the wave behavior under different ice covers. A companion paper (Part I) in this Proceedings details the 2013 HSVA experiment set up and data collection. The preliminary analysis is presented here to outline the procedure of inversely determining the parameters for a viscoelastic wave-ice model. A scaling law is proposed to connect laboratory data directly to field conditions.

Proceedings of the 22nd IAHR International Symposium on Ice

ISBN: 978-981-09-0750-1
doi:10.3850/978-981-09-0750-1_1224

1. Introduction

The motivation for a laboratory study of wave propagation in various ice covers is given in the companion paper (Part I). In which details of the data collection and types of ice cover are provided. In this paper we describe the preliminary data analysis. Three former laboratory studies are closely related to the present investigation. The first was a study of wave propagation through a grease ice field (Newyear and Martin 1999), in which it was found that the wave dispersion data agreed with a viscous layer model (Keller 1998). These data were used to inversely determine the effective viscosity of a grease ice layer. The second was a study of wave propagation through polyethylene sheets (Sakai and Hanai 2002). The total length of the polyethylene cover was kept the same but in each wave test the sheets were cut into successively smaller segments. It was found that by reducing the size of the segments without changing the overall dimension the wave speed was reduced. These data were used to fit with the thin elastic plate theory (e.g. Wadhams 1986). From which it was shown that the equivalent rigidity of the cover reduced with decreasing floe size. The third was a study of wave propagation through a grease/pancake ice field (Wang and Shen 2010a), where they propagated wave through a mixture of frazil and pancake ice field. They found that the viscous layer theory did not agree with the data, suggesting some rigidity parameter was missing. These three laboratory studies indicate that pure viscous model may not be sufficient to describe different ice cover types. A rigidity parameter, which might be floe size dependent, is also required. A viscoelastic model is a candidate because it allows for two parameters: the rigidity and the viscosity, to be included to determine the dispersion response (Wang and Shen 2010b). In the present paper, the 2013 HSVA data are used to illustrate the data processing and the inverse method to determine the rigidity and viscosity parameters from the measured dispersion data. Preliminary results are given. Full analysis will be conducted in the future. To save space, figures in Part I are not repeated here. Instead, when referred, they will be denoted as Fig. #-PI.

2. Experimental Data

In the 2013 HSVA experiment, there are two wave tanks shown in Fig.1-PI. Only sensors A, B, C, D, E, F, G, and 7 in tank 3 are used in this paper. Before the experiment, the voltage signals are calibrated with the water elevation. In the following sections the 'raw data' refers to the calibrated water elevation. The water depth on December 12 was 0.94m. The nominal depth of all sensors was at 0.24m. The sampling frequency was 100Hz, and the sampling period for each wave test was 60s, starting from the quiescent condition. A sample of the raw voltage data is shown in Fig. 1. Three types of ice covers were formed during the experiment: frazil/pancake ice, pancake ice, and fragmented ice. The ice thickness varied with time. Detailed information of the facility, the formation of ice and collection of experimental data can be found in Part I. In this paper we focus on one of such data sets taken on December 12 at 10:01 UTC. For this test the mean ice thickness was about 0.02m. The ice cover condition is shown in Fig. 1 (right).

3. Calculation of Wave Frequency

We select a range of 10s from the wave time series to calculate the wave frequency. In Wang and Shen (2010a), they employed four estimators to determine the wave frequency and found the differences among the methods were negligible. Therefore, we use one of the four methods, the

discrete Fourier transform (DFT) method in this study. First, we obtain the energy spectrum of the selected raw signal $s(n)$ as the following:

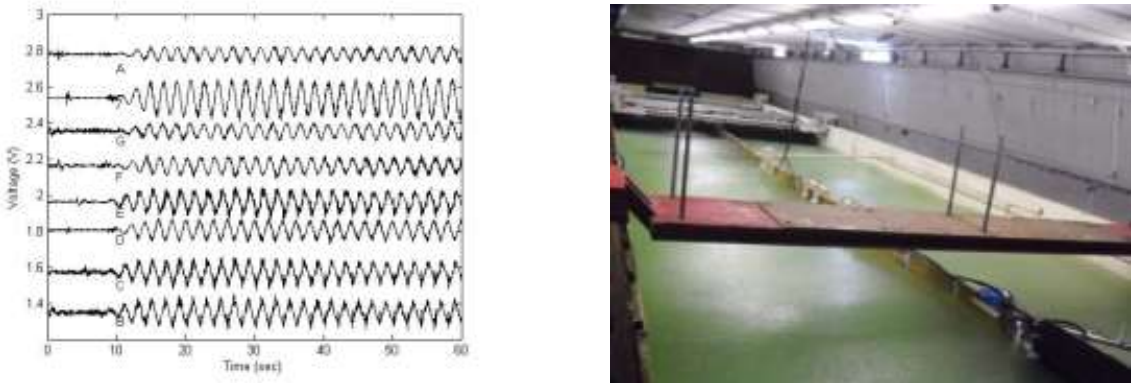

Figure 1. (Left) Sample time series in voltage. All data are displaced to aid visualization. (Right) the first frazil/pancake ice cover tested. Wave in tank 3 is visible.

$$S(f) = \frac{1}{L}\sum_{n=1}^{N} s(n)\exp(-2\pi i f t_n)\frac{L}{N} = \frac{1}{N}\sum_{n=1}^{N} s(n)\exp(-\frac{2\pi i f n L}{N}), t_n = \frac{nL}{N} \quad [1]$$

Here, L and N are the length and total number of the selected time series, f is frequency, and $S(f)$ is Fourier coefficient. The energy spectrum is defined as

$$E(f) = S(f)S^*(f) \quad [2]$$

The peak of the energy spectrum corresponds to the wave frequency. Figure 2 shows that the frequency for this data set is at 0.502 ± 0.0024Hz from all sensors.

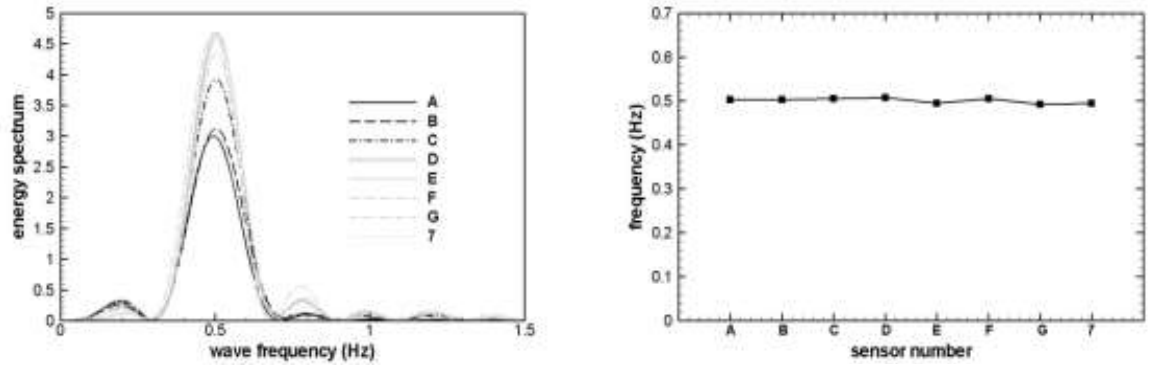

Figure 2. (Left) The energy spectrum and (Right) the frequency of the wave signal.

4. Calculation of Wave Number

To calculate the wave number k_r, we use the following equations:

$$c = \frac{\Delta l}{\Delta t}, \quad k_r = \frac{\omega}{c} \quad [3]$$

Here, c is the celerity, k_r is the wave number and $\omega = 2\pi f$ is the angular frequency. To obtain the celerity, distance between a chosen pair of sensors, Δl, and the time lag of the signal between this pair of sensors Δt are needed. The distances between sensors are given in Fig. 1-PI. To obtain the time lag, the time shift corresponding to the maximum of the correlation between signals from sensors a, b is determine. The time correlation function is calculated as:

$$C(\tau) = \int_0^L s_a(t)\, s_b(t+\tau) dt \qquad [4]$$

Figure 3(left) shows the time correlation function between three pairs of sensors. Between different pairs there is some difference in the time correlation. This variation may be reduced if filtered data are used. For the moment, we accept this variation. The resulting celerity between different pairs of sensors is given in Fig. 3(right). The mean and standard deviation of the celerity is 2.63 ± 0.22m/s. From Eq. [3], the resulting wave number is 1.20 ± 0.10m^{-1}.

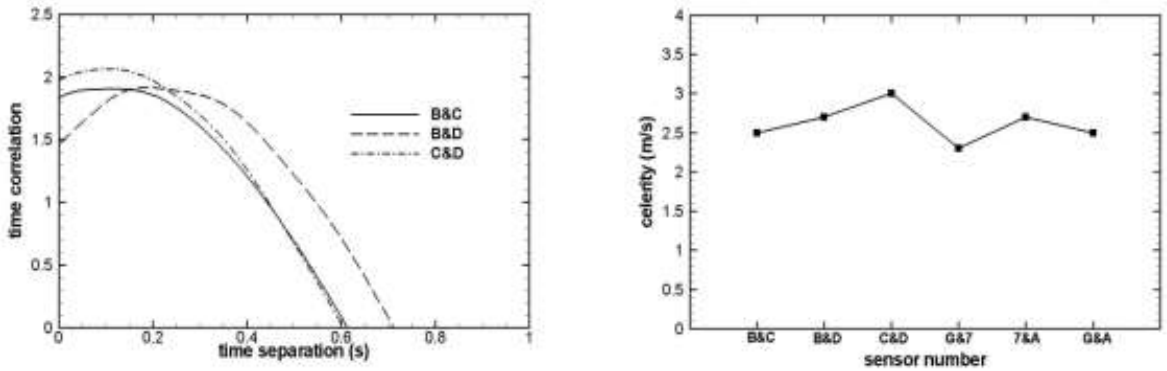

Figure 3. (Left) The time correlation and (Right) the celerity between two sensors.

5. Calculation of Wave Attenuation

For the wave attenuation calculation we assume that the wave has an exponential decay along the wave propagation direction. Thus, as in Wang and Shen (2010a), we use three pairs of sensors to calculate the attenuation coefficient:

$$k_i = \frac{\ln\left(\frac{a_G a_7 a_A}{a_B a_C a_D}\right)}{3l} \qquad [5]$$

where $a's$ represent amplitudes at the respective sensor locations and l is the distance between the center of sensor group $G, 7, A$ and B, C, D. During testing prior to the formation of ice covers, it was found that sensor A did not yield correct mean water level. However, its wave amplitude record was fine. Hence it is still included in Eq. [5] as well as in the celerity estimates mentioned above. To calculate the wave amplitude at each location, in the present study we use the DFT method again. As in section 3, we select 10s wave time series to calculate the amplitude for each sensor. The starting point of this 10s period for each sensor is based on the group velocity. The amplitude of the wave equals to the absolute value of the Fourier coefficient corresponding to the wave frequency. If we use the Matlab spectrum function as adopted in Wang and Shen (2010a) we found that the estimated wave amplitude is slightly lower than that from the DFT method.

For example at B the Matlab spectrum function yields 1.89cm, but the DFT method yields 1.95cm. These values are very close to each other. In addition, we are only interested in the ratio of the amplitudes at different locations. Hence the small difference between methods is not important. With this method we estimate the wave attenuation to be $0.0373 \pm 0.000043\text{m}^{-1}$.

6. Inverse Method for Estimation on Viscosity and Shear Modulus

Wang and Shen (2010b) proposed the viscoelastic sea ice model to generalize the viscous layer model and the thin elastic plate model. The dispersion relation for the ice-covered region has been obtained as shown below.

$$\omega^2 = (1 + \frac{\rho_{\text{ice}}}{\rho_{\text{water}}} \frac{\text{g}^2 k^2 S_k S_\alpha - (N^4 + 16k^6\alpha^2\nu_e^4)S_k S_\alpha - 8k^3\alpha\nu_e^2 N^2(C_k C_\alpha - 1)}{\text{g}k(4k^3\alpha\nu_e^2 S_k S_\alpha + N^2 C_k S_\alpha - \text{g}k S_k S_\alpha)})\text{g}k\tanh kH$$

$$\nu_e = \nu + \text{i}G/\rho_{\text{ice}}\omega,\ \alpha^2 = k^2 - \text{i}\omega/\nu_e \qquad [6]$$

where $S_k = \sinh kh$, $S_\alpha = \sinh \alpha h$, $C_k = \cosh kh$, $C_\alpha = \cosh \alpha h$, $N = \sigma + 2\text{i}k^2\nu_e$, h is the ice thickness, and H is the water depth. The equivalent mechanical properties of the ice cover are: ν the effective viscosity, and G the effective shear modulus. To complete this viscoelastic model, we need to parameterize ν and G for any given ice covers. To solve for ν and G under the present condition where the mean complex wave number $k = k_r + ik_i$ =1.20+i0.0373, we substitute $h = 0.02\text{m}$, $H = 0.94\text{m}$,$\omega = 3.14\text{Hz}$,$\rho_{ice} = 917\text{kgm}^{-3}$, and $\rho_{water} = 1032\text{kgm}^{-3}$ into Eq. [6] and plot the contours of the residual defined as the difference between the left and right side of Eq. [6]. These contours are shown Fig. 4. In this figure, there are two roots and one pole. The two roots give us the estimated ν and G which correspond to the measured wave number k_r and the attenuation k_i as shown in Table 1.

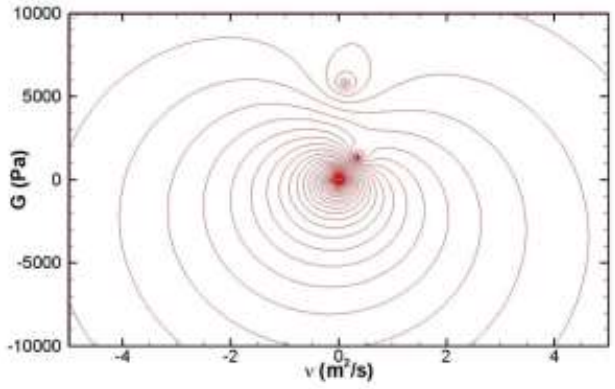

Figure 4. The contours of viscoelastic model dispersion relation function with complex wave number equals to (1.25, 0.0373). $h = 0.02\text{m}$, $H = 0.94\text{m}$,$\omega = 3.14\text{Hz}$,$\rho_{ice} = 917\text{kgm}^{-3}$, and $\rho_{water} = 1032\text{kgm}^{-3}$.

Both roots are acceptable since they produce the same observed wave characteristics. These values show that the ice cover is practically pure viscous since both ranges of G are very low. But even for this low G value it does affect k. For other types of ice cover, the results may be different as we will discuss next.

Table 1. The solutions for viscosity and shear modulus by the inverse method.

ν (m^2s^{-1})	G (Pa)
0.14 ± 0.03	6368 ± 1045
0.16 ± 0.13	1486 ± 179.8

To investigate the effect of ice morphology, we next look into the fragmented ice cover. This case corresponds to a test conducted on December 13, 12:47UTC where the ice cover is shown in Fig. 5-PI(right). Using the identical procedure mentioned above, the results are compared to the frazil/pancake ice case in Table 2. It is observed that with increasing ice thickness and ice floe diameters the wave number reduces, and the attenuation, viscosity and shear modulus all increase.

Table 2. The comparison between Frazil/Pancake ice and Fragmented ice cover.

Wave/Ice Parameters	Frazil/Pancake Ice	Fragmented Ice
Frequency (Hz)	0.502	0.498
Wave number (m^{-1})	1.20	0.95
Attenuation (m^{-1})	0.0373	0.0744
Ice Thickness (cm)	2	7
Ice Diameter (cm)	2	20
Viscosity (m^2s^{-1})	0.14	0.54
Shear Modulus (Pa)	6368	9846

7. Discussion and Conclusions

The above preliminary study gave an example of using measured data to inversely determine the parameters for a wave propagation model. Much more work is needed to establish a complete empirical formula that can relate the ice cover morphology to the equivalent viscoelastic properties. The example given shows at least two challenges exist. One is the uncertainty of measured data. Even a small variation in wave speed or attenuation contribute to a large range of the estimated G and ν. This phenomenon could mean that the viscoelastic parameters indeed do not have strong influence on the dispersion relation in some frequency ranges. A careful sensitivity analysis of the dispersion relation on its parameters is needed to this end. The other challenge is that there are multiple solutions of G and ν for each measured k. At this moment, we expect that other physical constraints will be available to select from one most reasonable solution.

Aside from parameterizing a viscoelastic model for wave propagation in ice covers, laboratory experiment may also be directly scaled up to field conditions. To do so, a dimensional analysis is required. Considering the process of wave-ice interaction, the key parameters needed are the change of the wave number and its amplitude, which are combined in the complex wave number $k = k_r + ik_i$. Let k_0 be the wave number in open water before entering the ice cover, we expect on physical grounds that

$$\tilde{k} = \frac{k}{k_0} = f(T, D, h, G_{ice}, \nu_m, \rho_{ice}, \rho_{water}, c) \quad [7]$$

In the above, the unknown function f depends on the wave period T, ice floe size D, ice cover thickness h, the shear modulus G_{ice} of individual ice floes, the viscous parameter ν_m, densities of ice ρ_{ice} and water ρ_{water}, and ice concentration c. The water depth H could be an important parameter only in shallow water cases. The viscous parameter can be the true viscosity of the fluid phase between ice floes, or the boundary layer effect under the floes, or a number of other fluid related dissipation mechanisms. The hysteresis effect from the floe themselves is conceivably another source of this viscosity parameter. A systematic study of these dissipation mechanisms is absent. Some conceptual work, focusing mainly on floe-floe collisions, can be found in Shen and Squire (1998). Our present consideration is to restrict ν_m to dissipation in the fluid phase only. Hence ν_m is physically different from ν the equivalent viscous parameter of the ice cover itself. If we choose h as the characteristic length, we may scale the parameters in the following way

$$\tilde{T} = T\sqrt{\frac{g}{h}}, \tilde{D} = \frac{D}{h}, \tilde{G} = \frac{G_{ice}}{\rho_{ice} g h}, \tilde{\nu}_m = \frac{\nu_m}{\sqrt{g h^3}}, \tilde{\rho} = \frac{\rho_{ice}}{\rho_{water}} \quad [8]$$

As long as the dimensionless parameters indicated by tilde are kept the same, the laboratory results should be directly convertible to field conditions. For instance, in the present laboratory case, $\tilde{\rho}$ may be considered as the same as in the field. Let $T_{lab} = 1\text{s}, D_{lab} = 10\text{cm}, h_{lab} = 2\text{cm}, G_{lab} = 10^5\text{Pa}, \nu_{m_{lab}} = 10^{-4}\text{cm}^2\text{s}^{-1}$, the measured $\tilde{k}$ should be the same as in the field for $T = 5\text{s}, D = 2.5\text{m}, h = 0.5\text{m}, G_{ice} \sim 2.5 \times 10^6\text{Pa}, \nu_m = 1.25 \times 10^{-2}\text{cm}^2\text{s}^{-1}$ provided that the ice concentrations in both cases are the same. The above is only one of many possible scaling laws. A proper choice of the scaling law depends on more physical knowledge of the processes underlying wave-ice interactions.

Acknowledgments

The work described in this publication was supported by the European Community's 7th Framework Programme through the grant to the budget of the Integrated Infrastructure Initiative HYDRALAB-IV, Contract no. 261520. The author(s) would like to thank the Hamburg Ship Model Basin (HSVA), especially the ice tank crew, for the hospitality, technical and scientific support and the professional execution of the test programme in the Research Infrastructure ARCTECLAB This work is supported in part by the Office of Naval Research Grant #N00014-13-1-0294.

References

Callinan C, Evers K U, Wilkinson J, Shen H H., 2014. Wave Propagation in Frazil/Pancake and Fragmented Ice Covers – Part I [C]. Proceedings of the 22th IAHR International Symposium on Ice. 2014: paper-225.

Keller, J.B., 1998. Gravity waves on ice-covered water, J. Geophy. Res., 103(C4):7663–7669.

Newyear, K., and Martin, S., 1999. Comparison of laboratory data with a viscous two-layer model of wave propagation in grease ice, J. Geophys. Res., 104(C4):7837-7840.

Sakai, S., and Hanai, K., 2002. Empirical formula of dispersion relation of waves in sea ice, In: Squire, V. A. and P. J. Langhorne (Eds), Ice in the Environment: Proc. 16th Inter. Symp. on Ice, vol. 2. Inter. Asso. Hydraulic Eng. & Res., Dunedin, New Zealand, 327-335.

Shen, H.H. and Squire, V.A., 1998. Wave Damping in Compact Pancake Ice Fields Due to Interactions Between Pancakes, AGU Antarctic Research Series 74, Antarctic Sea Ice: Physical Processes, Interactions and Variability, (Ed. Dr. Martin O. Jeffries): 325-342.

Wadhams, P., 1986. The seasonal ice zone, In Untersteier N, The Geophysics of sea ice, Plenum New York, 825-991.

Wang, R. and Shen, H.H, 2010a. Experimental study on surface wave propagating through a grease-pancake ice mixture. Cold Regions Science and Technology, 2010, 61: 90-96.

Wang, R. and Shen, H.H., 2010b. Gravity waves propagating into ice-covered ocean: a visco-elastic model, J. Geophy. Res., 115: C06024, doi:10.1029/2009JC005591.